Pergamon

Int. J. Solids Structures Vol. 35, Nos 9–10, pp. 761–782, 1998

0020–7683/98 $19.00 + .00

PII: S0020–7683(97)00084–X

DYNAMIC MODE III FRACTURE IN VISCOELASTIC MEDIA

P. H. GEUBELLE, M. J. DANYLUK and H. H. HILTON
Department of Aeronautical and Astronautical Engineering, University of Illinois, 104 South Wright Street, 306 Talbot Lab., MC-236, Urbana, IL 61801-2935, U.S.A.

(*Received* 18 *April* 1996; *in revised form* 27 *February* 1997)

Abstract—A spectral scheme for viscoelastodynamic fracture problems in anti-plane shear (mode III) loading conditions is presented. The numerical method is based on a spectral representation of the exact viscoelastodynamic relations between tractions and displacement discontinuities along the fracture plane. It allows for a precise and efficient investigation of dynamically loaded stationary or propagating cracks or faults in a viscoelastic medium, and incorporates a wide range of cohesive models used to characterize the failure process in the vicinity of the propagating crack tip. Various viscoelastodynamic fracture problems involving stationary and moving cracks are presented and contrasted with their elastic counterparts. © 1997 Elsevier Science Ltd.

1. INTRODUCTION

When a crack or a fault propagates dynamically in a linearly elastic material, the strain energy released by the crack advance is spent in the form of elastic waves and in the creation of new surfaces. If the material is viscoelastic, part of the energy is dissipated by the surrounding medium. The relative importance of the energy transfer mechanisms depends on the time scales at which these mechanisms take place. Quantifying this "competition" between elastodynamic and dissipative effects is of prime interest in modelling the failure behavior of viscoelastic structures.

While a relatively large number of papers have been published on the dynamic failure of linearly elastic materials (Freund, 1990), limited information is available on the dynamic loading and/or rapid propagation of cracks in viscoelastic media. The first paper dedicated to the viscoelastic effect on dynamic fracture mechanics was written by Willis (1967) who investigated the steady-state motion of a semi-infinite crack under anti-plane shear conditions in a standard linear solid. This pioneering work was extended by Walton (1982) to a more general class of viscoelastic materials. The problem of steady-state propagation of a crack in a viscoelastic material has also been the focus of Atkinson and Popelar, who considered dynamic crack propagation in a viscoelastic strip under both anti-plane shear (Atkinson and Popelar, 1979) and tensile loading (Popelar and Atkinson, 1980) conditions. This type of analysis has also been extended to the nonhomogeneous case (Herrmann and Schovanec, 1994) and the delamination problem (Sills and Benveniste, 1981; Ryvkin and Banks-Sills, 1994).

Due to the complexity of the relations involved, very few transient viscoelastodynamic results have been obtained so far. Most transient problems solved to date involve the idealized two-dimensional case of a semi-infinite crack that suddenly begins to propagate at a constant velocity under anti-plane shear (Atkinson and List, 1972; Herrmann and Walton, 1991) or tensile loading (Goleniewski, 1988; Herrmann and Walton, 1994). The transient problem of an accelerating semi-infinite crack under anti-plane shear conditions has also been investigated by Bourne and Walton (1993) based on a method developed earlier by Walton and Herrmann (1992). They were able to obtain a closed-form expression of the resulting space-time integral formulation of the viscoelastodynamic problem for the Achenbach–Chao class of viscoelastic materials. These recent developments are presented in

a paper by Walton (1995), together with a review of previous work on dynamic viscoelastic fracture mechanics.

A different type of viscoelastodynamic fracture problems has been recently investigated by Georgiadis *et al.* (1991) and Georgiadis (1993) who have presented a method to analyze the behavior of stationary cracks under a variety of dynamic loading conditions (anti-plane shear, torsional and plane loading). The method presented there is based on the correspondence principle and extends to the viscoelastic situation the integral transform method used by Chen and Sih (1977) to obtain the evolution of the dynamic stress intensity factor for various linearly elastic problems. The final step of the analysis, involving an inverse Laplace transform, was performed numerically.

As it has been alluded above, most of the analytical solutions involving the propagation of fast cracks in viscoelastic media have dealt with simplified geometries (semi-infinite cracks), loading conditions (2D anti-plane shear or tensile loading) and crack motion (steady-state or instantaneous acceleration). The complexity associated with the time-dependent material behavior precludes the analytical treatment of more complex situations involving finite-size 2D and 3D planar cracks subjected to any time-dependent mixed-mode loading conditions and propagating (or arresting) spontaneously. The objective in this series of papers is to develop an efficient numerical scheme that is able to tackle a wide variety of 2D and 3D viscoelastodynamic fracture problems.

In a recent paper, Geubelle and Rice (1995) have presented a spectral scheme for 3D dynamic fracture problems in homogeneous linearly elastic solids. The numerical scheme, which incorporates any combination of the three fracture modes, allows for an efficient and precise investigation of a wide range of problems involving the dynamic loading and/or rapid propagation of planar cracks and faults of arbitrary shapes in a homogeneous linearly elastic infinite body. The spectral formulation, which embodies an exact elastodynamic representation of the relation between the Fourier coefficients of the traction stresses on the fracture plane and the corresponding displacement discontinuities, is the 3D extension of an earlier anti-plane 2D formulation used by Perrin *et al.* (1994) to investigate the dynamic effects associated with various friction laws. The numerical characteristics of the anti-plane elastic spectral scheme have been reviewed by Morrissey and Geubelle (1997), who also showed how the numerical procedure can be used to simply and accurately extract the dynamic stress intensity factor.

This numerical scheme is based on a special formulation of the elastodynamic relation existing between the traction stress along the fracture plane and the associated displacement discontinuities. The formulation involves a convolution term which is expressed in the spectral domain as a time convolution over the past displacement (or velocity) history. The relation between the real (spatial) and spectral domains is obtained efficiently through a FFT algorithm. The phenomena associated with dynamic crack propagation can be investigated by combining the spectral scheme with any type of cohesive relations used to simulate the failure of the material on the fracture plane, ranging from simple linear cohesive laws (Geubelle and Rice, 1995) to more complex rate- and state-dependent friction models (Perrin *et al.*, 1994).

Since most viscoelastic problems are precisely characterized by the presence of time-convolution integrals associated with the integral representation of the time-dependent material behavior, this numerical scheme is particularly suited to investigate viscoelastodynamic problems: "all that is needed" is to combine the viscoelastic and elastodynamic effects in a single convolution kernel. However, the incorporation of the viscoelastic effect in the spectral formulation is somewhat more involved and the viscoelastodynamic formulation presents some major differences from the linearly elastic situation. The objective of this paper is to summarize these differences in the simpler anti-plane shear case, which despite its relative simplicity, contains most of the characteristics of the more complex fully 3D viscoelastic problem.

In the next section, a description of the mode III dynamic fracture problem is provided, followed by the basic relations used to characterize the surrounding viscoelastic medium. Then, the main steps leading to the derivation of the spectral form of the viscoelastodynamic equations and the associated numerical implementation are summarized in Section 3. Section 4 contains validation problems assessing the precision and stability of the numerical

scheme. Finally, fracture problems involving non-moving and moving cracks in viscoelastic media are presented and contrasted with elastic analyses in Sections 5 and 6, respectively.

2. PROBLEM AND MATERIAL DESCRIPTION

The objective of this paper is to develop an efficient numerical scheme to study the various dynamic fracture phenomena associated with the dynamic loading and/or the rapid propagation of a finite size planar crack in infinite viscoelastic homogeneous materials. Let the Cartesian coordinate system (x_1, x_2, x_3) be chosen such that the fracture plane is denoted by $x_2 = 0$. Since the present paper is concerned exclusively with the 2D anti-plane shear problem, it is assumed that all field quantities are independent of x_3, and we denote the sole displacement component in the x_3-direction by $w(x_1, x_2, t)$. The viscoelastodynamic fracture problem to be solved numerically with the spectral scheme described hereafter can be summarized as follows: starting at time $t = 0$, a space- and time-dependent anti-plane shear loading $\tau_3^0(x_1, t)$ is suddenly applied on the initially stress-free and quiescent fracture plane. The externally applied loading generates a displacement discontinuity across the portion of the fracture plane where the pre-existing flaw was located. As the crack opens, dynamic stresses build up in the vicinity of the crack tips. When the traction stress exceeds the failure strength of the surrounding viscoelastic medium, the crack starts to propagate spontaneously. The failure process of the surrounding material is assumed to be constrained to the fracture plane and is incorporated in the numerical scheme through a very general cohesive law. Since the size of the crack and, thereby, the problem geometry evolve *spontaneously* (i.e., are part of the solution itself), this class of dynamic fracture problems is inherently nonlinear and necessitates the use of a numerical tool, even in the simpler case of 2D anti-plane shear loading conditions. Even when the failure strength of the surrounding medium is too high to allow for any propagation of the pre-existing flaw, the solution will be characterized by a highly complex transient wave pattern which also precludes a purely analytical treatment, especially in the viscoelastic situation considered in this work.

Before deriving the major steps leading to the spectral form of the integral equation which serves as the basis for the numerical scheme proposed hereafter, let us summarize the material description used in this paper.

Let $\varepsilon_{\alpha 3} = w_{,\alpha}/2$ $(\alpha = 1, 2)$ be the non-vanishing strain components related to the corresponding stress components $\sigma_{\alpha 3}$ through the conventional general viscoelastic differential form of the constitutive relations

$$P\{\sigma_{\alpha 3}(x_\beta, t)\} = 2\mu_o Q\{\varepsilon_{\alpha 3}(x_\beta, t)\} \tag{1}$$

where μ_o is a normalizing factor with stress dimensions, while P and Q are differential operators expressed as

$$P = \sum_{n=0}^{r} a_n \frac{\partial^n}{\partial t^n}; \quad Q = \sum_{n=0}^{s} c_n \frac{\partial^n}{\partial t^n}. \tag{2}$$

By introducing the Laplace transform

$$\hat{f}(p) = \mathscr{L}[f(t)] = \int_0^\infty f(t)\, e^{-pt}\, \mathrm{d}t, \tag{3}$$

the constitutive relation (1) can be rewritten as

$$\hat{\sigma}_{\alpha 3}(x_\beta, p) = 2\mu_o \hat{m}(p) \hat{\varepsilon}_{\alpha 3}(x_\beta, p), \tag{4}$$

where $\hat{m}(p)$ is the dimensionless Laplace transform shear modulus given by

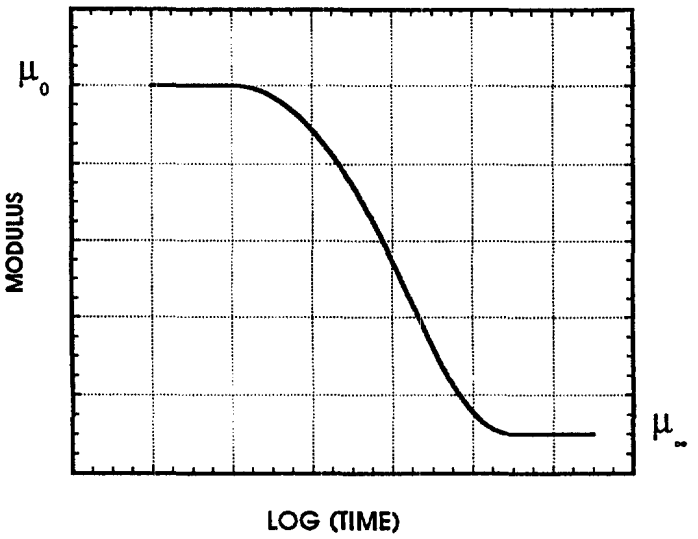

Fig. 1. Schematic evolution of the relaxation shear modulus.

$$\hat{m}(p) = \frac{\hat{Q}(p)}{\hat{P}(p)} = \frac{\sum_{n=0}^{s} c_n p^n}{\sum_{n=0}^{r} a_n p^n}. \tag{5}$$

When $r = s = N$ as is the case for solids, μ_o is the instantaneous (elastic) shear modulus, and the relaxation modulus in shear can be expressed, after reduction to partial fractions, as a sum of exponential terms in the time domain,

$$\mu(t) = \mu_o \mathscr{L}^{-1}\left[\frac{\hat{m}(p)}{p}\right] = \mu_\infty + \sum_{n=1}^{N} \mu_n e^{-t/\tau_n}, \tag{6}$$

where μ_∞ is the fully relaxed shear modulus and N and τ_n are related to material properties (Hilton, 1964). A schematic of the evolution of the relaxation shear modulus is presented in Fig. 1. The instantaneous modulus is then given by

$$\mu_o = \mu_\infty + \sum_{n=1}^{N} \mu_n. \tag{7}$$

3. SPECTRAL FORMULATION AND NUMERICAL IMPLEMENTATION

The basic derivation of the spectral formulation of viscoelastodynamic problems is somewhat similar to that of the elastodynamic case described in Perrin *et al.* (1994) and in Geubelle and Rice (1995). For completeness purposes, the main steps of the viscoelastic derivation are summarized here.

The out-of-plane displacement $w(x_1, x_2, t)$ satisfies, on the (x_1, x_2) plane, the viscoelastic wave equation

$$Q\left\{\frac{\partial^2 w}{\partial x_1^2} + \frac{\partial^2 w}{\partial x_2^2}\right\} = \frac{\rho}{\mu_o} P\left\{\frac{\partial^2 w}{\partial t^2}\right\}, \tag{8}$$

where the operators P and Q have been introduced in (1), and ρ is the constant mass density of the material. In preparation for a Fourier series approximation of the solution, we examine a single spectral mode

$$w(x_1, x_2, t) = \Omega(x_2, t; q) \exp(iqx_1) \tag{9}$$

and rewrite the wave eqn (8) as

$$\hat{\Omega}''(x_2, p; q) = q^2 \hat{\alpha}_s^2(p; q) \hat{\Omega}(x_2, p; q), \tag{10}$$

where the primes denote differentiation with respect to x_2 and

$$\hat{\alpha}_s(p; q) = \sqrt{1 + \frac{p^2}{q^2 \hat{c}_s^2(p)}}. \tag{11}$$

In the latter relation, we choose the complex square root to have a non-negative real part, while $\hat{c}_s(p)$ is the Laplace transform shear wave speed and is given by

$$\hat{c}_s^2(p) = \frac{\mu_o}{\rho} \hat{m}(p) = c_{so}^2 \hat{m}(p), \tag{12}$$

where $c_{so} = \sqrt{\mu_o/\rho}$ is the shear wave velocity corresponding to the initial modulus and will be used throughout the present analysis as the reference shear wave speed. The solution to (10) for the upper plane ($x_2 > 0$) is

$$\hat{\Omega}(x_2, p; q) = \hat{W}(p; q) \exp(-|q| \hat{\alpha}_s(p; q) x_2). \tag{13}$$

Let $\tau_3(x_1, t)$ denote the traction stress along the fracture plane as

$$\tau_3(x_1, t) = \sigma_{23}(x_1, 0, t) = T(t; q) \exp(iqx_1). \tag{14}$$

Using the constitutive relations (4) and the displacement solution (13), one can express the Fourier coefficients of the traction stress $T(t; q)$ along the fracture plane as

$$\hat{T}(p; q) = \mu_o \hat{m}(p) \left[\frac{\partial \hat{\Omega}(x_2, p; q)}{\partial x_2} \right]_{x_2 = 0} = -\frac{1}{2} |q| \hat{\alpha}_s(p; q) \mu_o \hat{m}(p) \hat{D}(p; q), \tag{15}$$

where $D(t; q)$ is the Fourier coefficient of the displacement jump $\delta(x_1, t)$ across the fracture plane defined as

$$\delta(x_1, t) = w(x_1, 0^+, t) - w(x_1, 0^-, t) = D(t; q) \exp(iqx_1). \tag{16}$$

At this point, the instantaneous response is extracted as

$$[\tau(x_1, t)]_{inst} = -\frac{\mu_o}{2c_{so}} \dot{\delta}(x_1, t), \tag{17}$$

where the dot denotes differentiation with respect to time. The solution (15) is then rewritten as

$$\hat{T}(p; q) = -\frac{\mu_o}{2c_{so}} p \hat{D}(p; q) - \frac{|q| \mu_o}{2} \left[\hat{\alpha}_s(p; q) \hat{m}(p) - \frac{p}{|q| c_{so}} \right] \hat{D}(p; q), \tag{18}$$

where the expression of $\hat{\alpha}_s(p; q)$ is obtained by combining (11) and (12).

In the time domain, (18) becomes

$$\tau_3(x_1,t) = \tau_3^0(x_1,t) - \frac{\mu_o}{2c_{so}}\dot{\delta}(x_1,t) + \bar{f}(x_1,t), \tag{19}$$

where the externally applied traction stress $\tau_3^0(x_1,t)$ (associated, for example, with the arrival of a plane wave) has been added and where $\bar{f}(x_1,t)$ is a convolution term, the Fourier coefficient of which is given by a convolution over the past displacement history as

$$\bar{F}(t;q) = -\frac{\mu_o|q|}{2}\int_0^t R_{\mathrm{III}}^{ve}(|q|c_{so}t')D(t-t';q)|q|c_{so}\,\mathrm{d}t'. \tag{20}$$

The viscoelastic convolution kernel $R_{\mathrm{III}}^{ve}(T)$ appearing in (20) is the inverse Laplace transform of the bracketed term in (18).

The Laplace transform of the convolution kernel is quite complicated and its Laplace inversion must, in most cases, be performed numerically. Among the various algorithms available, the DAC method, named after Dubner, Abate and Crump (Dubner and Abate, 1968; Crump, 1976), has been shown to be particularly reliable and efficient and will be used in the present analysis. Details on the numerical Laplace inversion can be found in Georgiadis (1993).

The convolution kernel depends on the material parameters used to characterize the viscoelastic response (6). For the sake of illustration, the remainder of the spectral method presentation will focus on a simple viscoelastic model, the standard linear solid (SLS) model. The more general case involving a Prony series representation of the material response is described in the Appendix. The relaxation shear modulus for the SLS model is given by

$$\mu(t) = \frac{\mu_o}{1+\xi}\left[1+\xi\exp\left(-\frac{1+\xi}{\tau}t\right)\right], \tag{21}$$

where $\xi = [(\mu_o/\mu_\infty)-1]$ and $\tau/(1+\xi)$ is the (sole) relaxation time.

The corresponding Laplace transform dimensionless shear modulus defined by (5) is

$$\hat{m}(p) = \frac{p+1/\tau}{p+(1+\xi)/\tau}. \tag{22}$$

Substituting (22) into (11), (12) and (18), and defining $s = p/(|q|c_{so})$, one obtains

$$\mathscr{L}[R_{\mathrm{III}}^{ve}(T)] = \sqrt{1+s^2\left(1+\frac{b\xi}{s+b}\right)}\left(\frac{s+b}{s+b+b\xi}\right) - s, \tag{23}$$

where the nondimensional parameter b is given by

$$b = \frac{1}{|q|c_{so}\tau}, \tag{24}$$

and combines the effects of both the relaxation time τ and the mode number $|q|$. As will be discussed subsequently, this parameter plays a significant role in characterizing viscoelastic effects and strongly influences the precision and stability of the numerical scheme. Even for the simpler case of the SLS mode described here (and *a fortiori* for the more complex Prony series model described in the Appendix), a closed-form expression of the convolution kernel $R_{\mathrm{III}}^{ve}(T)$ is so far beyond reach, except in the elastic limit ($\xi = 0$ and/or $\tau \to \infty$) for which

$$R^{e}_{III}(T) = \mathscr{L}^{-1}[\sqrt{1+s^2}-s] = \frac{J_1(T)}{T}, \tag{25}$$

where $J_1(T)$ is the Bessel function of the first kind.

The DAC algorithm used for the numerical inversion requires that the Laplace-domain expression of the convolution kernel vanish for large values of s. Since

$$\lim_{s\to\infty}[\hat{R}^{ve}_{III}(s)] = -\frac{b\xi}{2}, \tag{26}$$

we rewrite the convolution kernel as

$$\hat{C}^{ve}_{III}(s;q) = \hat{R}^{ve}_{III}(s;q) + \frac{b\xi}{2} \tag{27}$$

to adequately capture its behavior at the origin.

The expression of the time-dependent Fourier coefficient of the convolution term is thus

$$\bar{F}(t;q) = \frac{\mu_o|q|}{4} b\xi D(t;q) - \frac{\mu_o|q|}{2}\int_0^t C^{ve}_{III}(|q|c_{so}t')D(t-t';q)|q|c_{so}\,dt', \tag{28}$$

where the Laplace transform of the kernel $C^{ve}_{III}(T)$ is obtained from (23) and (27). The numerically inverted convolution kernel $C^{ve}_{III}(T)$ is presented in Figs 2a and 2b for $\xi = 1$ and 10, respectively. By combining (24) and (28), we obtain the final spectral expression of the viscoelastodynamic equation on the fracture plane as

$$\tau_3(x_1,t) = \tau^0_3(x_1,t) - \frac{\mu_o}{2c_{so}}\dot{\delta}(x_1,t) + \frac{\mu_0\xi}{4c_{so}\tau}\delta(x_1,t) + f(x_1,t), \tag{29}$$

where the Fourier coefficient of the convolution term is now

$$F(t;q) = -\frac{\mu_o|q|}{2}\int_0^t C^{ve}_{III}(|q|c_{so}t')D(t-t';q)|q|c_{so}\,dt'. \tag{30}$$

Note the appearance of a new term on the right-hand side of (29): the term proportional to the displacement discontinuity is characteristic of the viscoelastic problem and vanishes in the elastic limit ($\xi = 0$ and/or $\tau \to \infty$).

The variation of $C^{ve}_{III}(T)$ shown in Fig. 2 suggests three important comments: firstly, unlike in the elastic case where all Fourier modes have the same kernel, the viscoelastic kernel strongly depends on the mode number $|q|$ through the parameter $b = 1/(|q|c_{so}\tau)$, such that every spatial mode will have a different convolution kernel. Secondly, as b becomes smaller (i.e., as $|q|$ and/or τ increase), the viscoelastodynamic kernel approaches its elastic counterpart $J_1(T)/T$. Finally, the convolution kernel experiences a severe drop for small values of its argument, especially for larger values of b. This fact is further illustrated on a logarithmic scale in Fig. 3.

The value of the convolution kernel at the origin is

$$C^{ve}_{III}(0) = \frac{1}{2}\left[1 + \left(\frac{3\xi^2}{4} + \xi\right)b^2\right]. \tag{31}$$

It increases rapidly with b and becomes unbounded as $b \to \infty$, i.e., as $q \to 0$ and/or $\tau \to 0$.

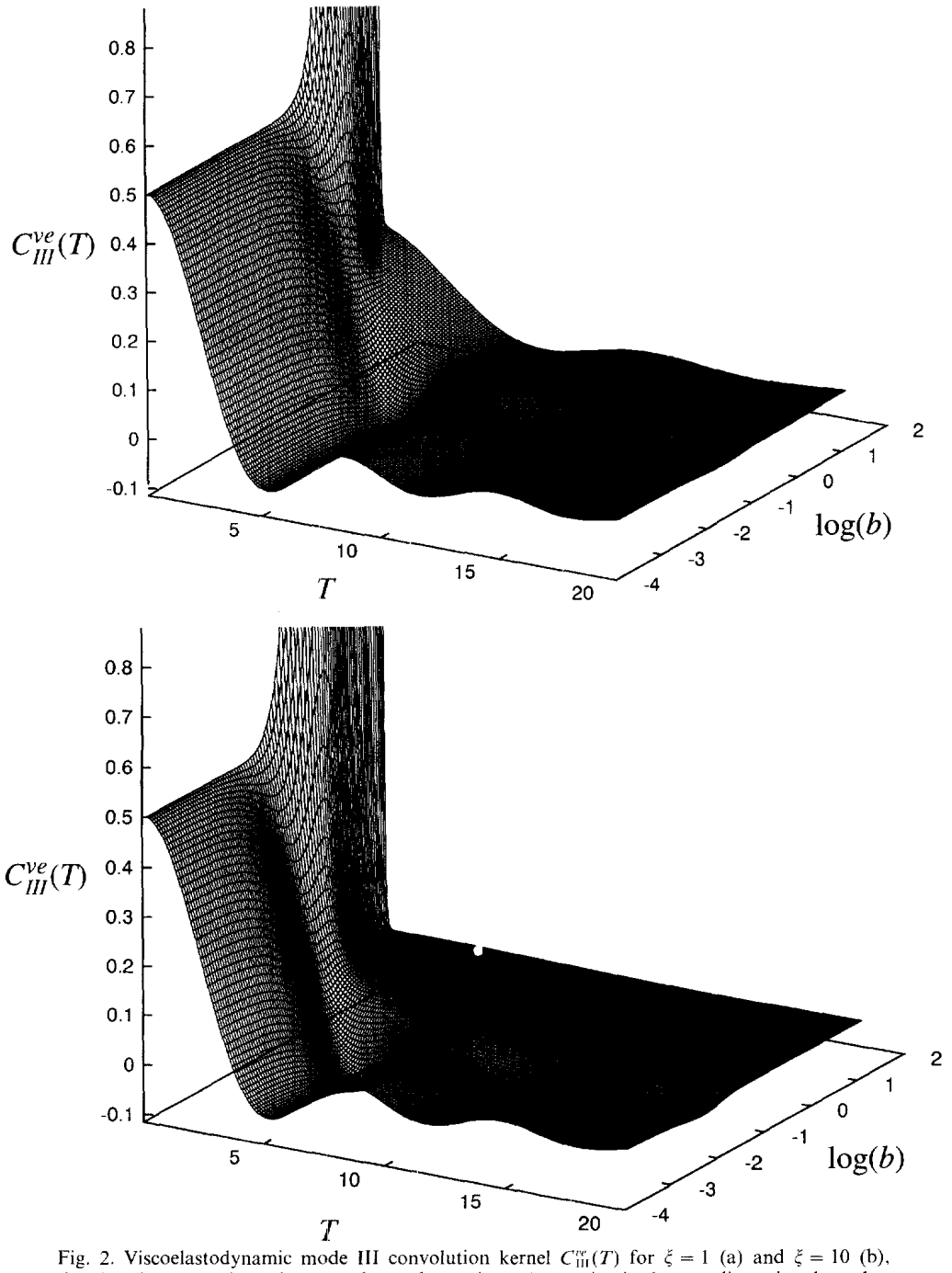

Fig. 2. Viscoelastodynamic mode III convolution kernel $C^{ve}_{III}(T)$ for $\xi = 1$ (a) and $\xi = 10$ (b), showing the strong dependence on the mode number q (appearing in the non-dimensional number $b = 1/|q|c_{so}\tau$).

The rapid variation of the kernel in the vicinity of the origin has an important consequence on the precision of the numerical scheme and will be investigated in the validation studies described in the next section. However, the unbounded initial value of the kernel for the constant mode ($q = 0$) creates a second major distinction between the elastic and viscoelastic problems. Since the unique (mode-independent) elastodynamic convolution kernel $J_1(T)/T$ is finite for all values of its argument, it is clear from (20) that the constant mode (i.e., corresponding to $q = 0$) does not at all contribute to the convolution term. In the viscoelastic case, however, the integrand tends to infinity, resulting in an indeterminate form which can only be removed by rewriting the viscoelastodynamic equation for the constant mode ($q = 0$).

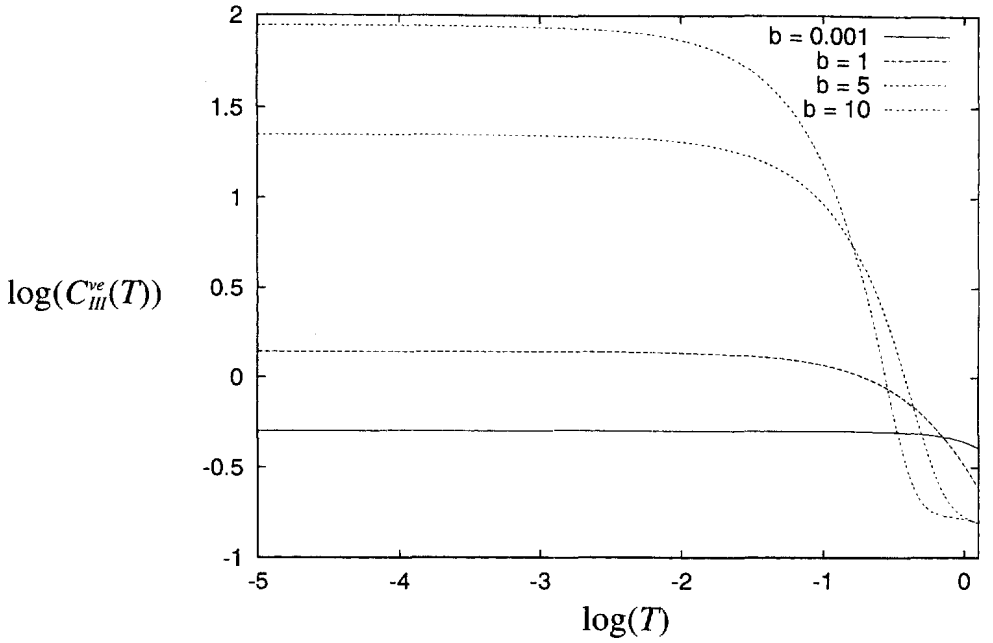

Fig. 3. Logarithmic variation of the convolution kernel with respect to T for $\xi = 1$ and for various values of b, showing a rapid variation near the origin.

By taking the limit of (18) as $q \to 0$, the Laplace-transform relation between the Fourier coefficients of the traction stress and the displacement jump for the constant mode becomes

$$\hat{T}(p;0) = -\frac{\mu_o}{2c_{so}} p\hat{D}(p;0) - \frac{\mu_o}{2c_{so}}\left[p\sqrt{\frac{p+1/\tau}{p+(1+\xi)/\tau}} - p\right]\hat{D}(p;0). \tag{32}$$

The bracketed term in (32) is the convolution kernel for the constant mode. Note that it vanishes in the elastic limit as described earlier. Following the same procedure as used in (26) and (27), the Fourier coefficient for the constant-mode convolution term can be shown to be

$$\bar{F}(t;0) = \frac{\mu_o}{4}\frac{\xi}{c_{so}\tau} D(t;0) - \frac{\mu_o}{2c_{so}\tau}\int_0^t C_o^{ve}\left(\frac{t'}{\tau}\right) D(t-t';0)\frac{\mathrm{d}t'}{\tau}, \tag{33}$$

where $C_o^{ve}(T)$ is the constant mode (0th spectral mode) convolution kernel given by

$$\begin{aligned} C_o^{ve}(T) &= \mathscr{L}^{-1}\left[s\sqrt{\frac{s+1}{s+1+\xi}} - s + \frac{\xi}{2}\right] \\ &= \frac{\xi}{2} e^{-[1+(\xi/2)]T}\left[(1+\xi)\left(I_o\left(\frac{\xi}{2}T\right) - I_1\left(\frac{\xi}{2}T\right)\right) - \frac{1}{t} I_1\left(\frac{\xi}{2}T\right)\right], \end{aligned} \tag{34}$$

where I_o and I_1 are modified Bessel functions. The constant mode convolution kernel is illustrated in Fig. 4 for various values of ξ.

The final form of the constant mode convolution term $f(x_1, t)$ to be used in (29) is obtained by subtracting the first term on the right-hand-side of (33) to yield

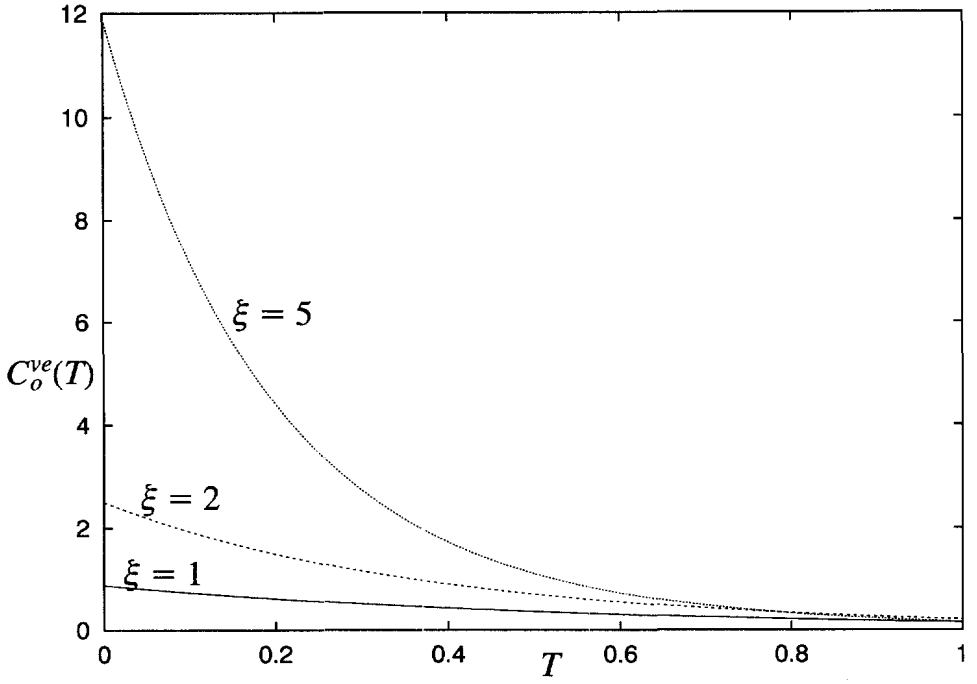

Fig. 4. Convolution kernel $C_o^{ve}(T)$ for the constant mode for various values of ξ.

$$F(t;0) = -\frac{\mu_o}{2c_{so}\tau}\int_0^t C_o^{ve}\left(\frac{t'}{\tau}\right) D(t-t',0)\frac{\mathrm{d}t'}{\tau}. \tag{35}$$

In conclusion, the spectral form of the relation between the viscoelastodynamic traction stress along the fracture plane and the corresponding crack opening displacements and velocities are given, for the SLC class of viscoelastic materials, by (29), (30) and (35), with the convolution kernels given by (23) and (27) for the non-zero modes, and by (34) for the constant mode. To complete the formulation and obtain the numerical implementation, the dynamic stress $\tau_3(x_1, t)$ is compared with the strength to determine whether failure occurs: if the absolute value of the dynamic stress at a particular location is inferior to the current local value of the strength, no failure takes place and no further opening of the crack is allowed. But if the dynamic stress exceeds the local value of the strength, the material fails at that location and the crack opening velocity $\dot{\delta}(x_1, t)$ is computed using (29) with the current value of the strength on the left-hand-side of the equation.

As the material fails, its strength deteriorates. One of the main advantages of the proposed numerical method is that it allows the incorporation of a wide range of cohesive models to describe the failure process. This cohesive model can be expressed in general form as a general relation between the strength S and the current and past values displacement and velocity, the location and the time, as in

$$S(x_1, t) = f(x_1, t, \delta, \dot{\delta}). \tag{36}$$

The numerical implementation of the spectral formulation is similar to that of the elastic problem described in detail by Geubelle and Rice (1995). It starts with the discretization of a portion X of the fracture plane into M equally spaced elements, defining a grid with uniform spacing $\Delta x = X/M$. The crack opening distribution $\delta(x_1, t)$ and the convolution term $f(x_1, t)$ are expressed in a Fourier series as

$$\begin{Bmatrix}\delta(x_1, t)\\ f(x_1, t)\end{Bmatrix} = \sum_{m=-M/2}^{M/2} \begin{Bmatrix}D_m(t)\\ F_m(t)\end{Bmatrix} \exp\left(\frac{2\pi i m x_1}{X}\right), \tag{37}$$

where the time-dependent Fourier coefficients $D_m(t)$ and $F_m(t)$ are related through (30) for

the non-zero modes and (35) for the constant mode. The value of the mode numbers q to be used in (30) can be found by direct comparison between (9) and (37). The transition between spectral and spatial domains is achieved very efficiently by using a FFT algorithm with the predefined grid points as sampling points. The convolution integrals appearing in (30) and (35) are evaluated numerically using a simple trapezoidal rule. Finally, an explicit time-integration scheme is used to compute displacement distributions from velocity distributions. Letting $g_{i,n} = g(i\Delta x, n\Delta t)$ denote the space- and time-discretized value of a function $g(x_1, t)$, we can summarize the algorithm for *rate-independent* cohesive models as follows:

(1) impose the initial conditions ($n = 0$) ($i = 1, \ldots, M$): $S_{i,0}$ and $\tau^o_{3i,0}$ known; $\delta_{i,0} = 0$
(2) compute the initial velocity distribution

$$\dot{\delta}_{i,0} = \frac{2c_{so}}{\mu_o} \operatorname{sign}(\tau^0_{3i,0}) \max(|\tau^0_{3i,0}| - S_{i,0}, 0)$$

(3) for each time step
  (3.1) update the crack opening displacement distribution:

$$\delta_{i,n} = \delta_{i,n-1} + \Delta t\, \dot{\delta}_{i,n-1}$$

  (3.2) update the applied stress $\tau^0_{3i,n}$ and the strength distribution $S_{i,n}$ based on the current position of the crack and current or past values of the displacement
  (3.3) perform a FFT on the current displacement distribution: $D_{i,n} = \mathrm{FFT}(\delta_{i,n})$
  (3.4) perform the convolution on the Fourier coefficients of the past displacement history with appropriate kernel to find the Fourier coefficients of the convolution term $F_{i,n}$
  (3.5) perform an inverse FFT to find the convolution term: $f_{i,n} = \mathrm{FFT}^{-1}(F_{i,n})$
  (3.6) compute the current dynamic stress distribution:

$$\tau_{di,n} = \tau^o_{3i,n} + \frac{\mu_o \xi}{4c_{so}\tau} \delta_{i,n} + f_{i,n}$$

  (3.7) compute the updated velocity distribution with (29) by comparing the dynamic stress and the strength:

$$\dot{\delta}_{i,n} = \frac{2c_{so}}{\mu_o} \operatorname{sign}(\tau_{di,n}) \max(|\tau_{di,n}| - S_{i,n}, 0).$$

If the cohesive model is *rate-dependent*, i.e., if the strength of the surrounding medium depends on the crack opening velocity in (36), the strength update (Step 3.2) and the velocity computation (Step 3.7) have to be performed simultaneously. Note that the difference between the cracked and the uncracked portions of the fracture plane is simply determined by comparing the current value of the dynamic stress with that of the strength: failure will take place where the dynamic stress exceeds the strength. The crack corresponds to the region for which the material has completely failed, and the strength is down to zero.

As emphasized by Geubelle and Rice (1995), the main advantages of the spectral scheme are its simplicity, its efficiency and its easy adaptability to massively parallel computers. It however suffers from two limitations associated with the use of the Fourier series representation (37) of the solution. The first one is the artificial spatial replication of the fracture event on the fracture plane. This issue has been addressed in a recent paper by Cochard and Rice (1996) who have eliminated the periodicity while maintaining the spectral form of the elastodynamic relations by taking X equal to twice the size of the crack, and by introducing a slightly different convolution kernel. The second problem is the possible appearance of a numerical imprecision associated with finite Fourier series representation of functions with non-vanishing spectral content (Gibbs phenomenon). This effect was

however shown to be in most cases very limited and could be avoided through the use of more advanced uniformly convergent spectral methods (Gottlieb *et al.*, 1992).

The next section describes validation examples used to characterize the precision and stability of the developed scheme.

4. VALIDATION OF THE NUMERICAL SCHEME: MODAL ANALYSIS

The modal analysis consists of investigating the dynamic response of a single spectral mode to a sudden step-like loading. The strength on the whole fracture plane is assumed to be zero. This method was introduced by Geubelle and Rice (1995) to investigate the precision of the linearly elastic spectral scheme in mode I, and later used by Morrissey and Geubelle (1997) to characterize elastodynamic mode III solutions. The advantages of this analysis are twofold: Firstly, it allows one to extract from the total numerical error associated with the spectral scheme the imprecision associated with the forward and backward FFT. Secondly, it allows one to precisely quantify the error associated with each mode q appearing in the Fourier series representation of the displacement distribution (37) and with the choice of time step Δt used to calculate the crack opening along the fracture plane using the velocity distribution.

Let the externally applied traction stress on the fracture plane by given by

$$\tau_3^o(x_1, t) = T_o H(t) \exp(iqx_1), \tag{38}$$

where $H(t)$ is the Heaviside step function. Combining (15) and (38), the corresponding velocity response for non-zero modes ($q \neq 0$) in the Laplace domain becomes

$$p\hat{D}(p; q) = \frac{2T_o}{|q|\mu_o \hat{m}(p)\hat{\alpha}_s(p; q)}. \tag{39}$$

In the time domain, the opening velocity can be expressed in nondimensional form as

$$r(t) = \frac{\dot{D}(t)}{\dot{D}(0)} = \frac{\mu_o \dot{D}(t)}{2c_{so}T_o} = g(|q|c_{so}t), \tag{40}$$

where with the aid of (11) and (12)

$$g(T) = \mathscr{L}^{-1}\left[\frac{s+(1+\xi)b}{\sqrt{(s+n)(s^3+(1+\xi)bs^2+s+b}}\right], \tag{41}$$

with the nondimensional parameter b defined in (24). The analytical solution of the modal problem, expressed by (40) and (41), is obtained by a numerical Laplace transform inversion using the aforementioned DAC technique and is shown in Fig. 5. Note that in the linearly elastic case, $\xi = 0$ or $\tau \to \infty$, the nondimensional velocity (40) becomes $r(t) = J_o(|q|c_s t)$ (Morrissey and Geubelle, 1997).

Figure 5 illustrates the competition between viscoelastic effects, which tend to decrease the shear modulus resulting in an increased velocity response and the elastodynamic effects, which lead to oscillatory velocity responses of decreasing amplitude (as illustrated by the elastic solution represented by the solid curve in Fig. 5). As emphasized in the semi-logarithmic plot given in the insert of Fig. 5, the initial response is greatly influenced by the material relaxation behavior. For large values of τ (i.e., small values of b), elastodynamic effects have more influence on the solution than viscoelastic effects. For smaller values of τ (i.e., large values of b), the opposite is true due to material relaxation. Thus, for smaller values of τ, the velocity response initially increases, as a result of relaxation, before the elastodynamic effects bring the solution to zero. This competition between the viscoelastic and dynamic effects is also characteristic of the way in which the velocity "dies out" for large times. The modal solution shows a distinct transition between the two limiting

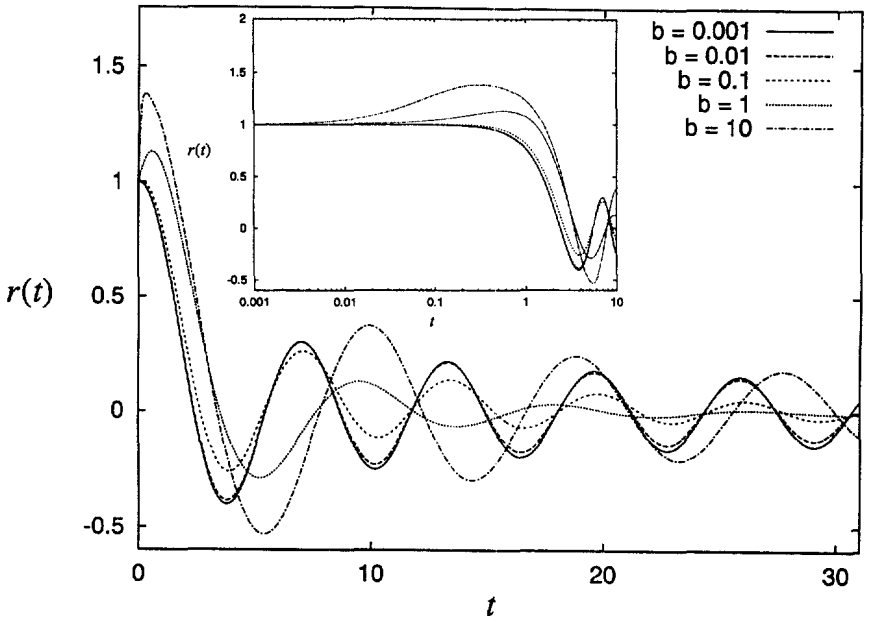

Fig. 5. Exact solution of the modal problem for $\xi = 1$ and for various values of b. The insert shows the small-time solution on a semi-logarithmic scale.

elastic solutions: The first one corresponds to the initial modulus μ_o and is given by $r(t) = J_o(|q|c_s t)$; the second elastic solution is associated with the fully relaxed modulus μ_∞ and is expressed as $r(t) = \sqrt{1+\xi} J_o(\sqrt{1+\xi}|q|c_s t)$. For intermediate values of b ($b \approx 1$), the solution experiences rapid damping, which could readily be seen from the variation of the viscoelastodynamic convolution kernel in Fig. 2.

The numerical implementation of the spectral scheme takes a very simple form in the modal analysis. Let the discrete nondimensional crack opening displacement be defined by

$$d_n = \frac{D(n\Delta t)}{\dot{D}(0)\,\Delta t}, \tag{42}$$

where Δt is the time step used in the time integration scheme. The convolution integral (30) is discretized using the trapezoidal rule, yielding, with the aid of (29) and (42),

$$r_n = r(n\Delta t) = 1 + \frac{\gamma b \xi}{2} d_n - \gamma^2 \sum_{j=1}^{n} Q_j d_{n+1-j}, \tag{43}$$

where $\gamma = |q|c_{so}\Delta t$, and

$$Q_j = \tfrac{1}{2}[C^{ve}_{\mathrm{III}}((j-1)\gamma) + C^{ve}_{\mathrm{III}}(j\gamma)]. \tag{44}$$

In the elastic case, γ is the only parameter needed to quantify the effects of both the time step Δt and the mode number q on the precision and stability of the numerical scheme (Geubelle and Rice, 1995). In the viscoelastic case, two parameters are needed, γ and b. Note that one can isolate the effect of the time step Δt by comparing it with the material related time constant τ as

$$\zeta = \gamma b = \frac{\Delta t}{\tau}. \tag{45}$$

The numerical formulation of the modal problem is completed by an explicit time integration scheme, written in a nondimensional form as

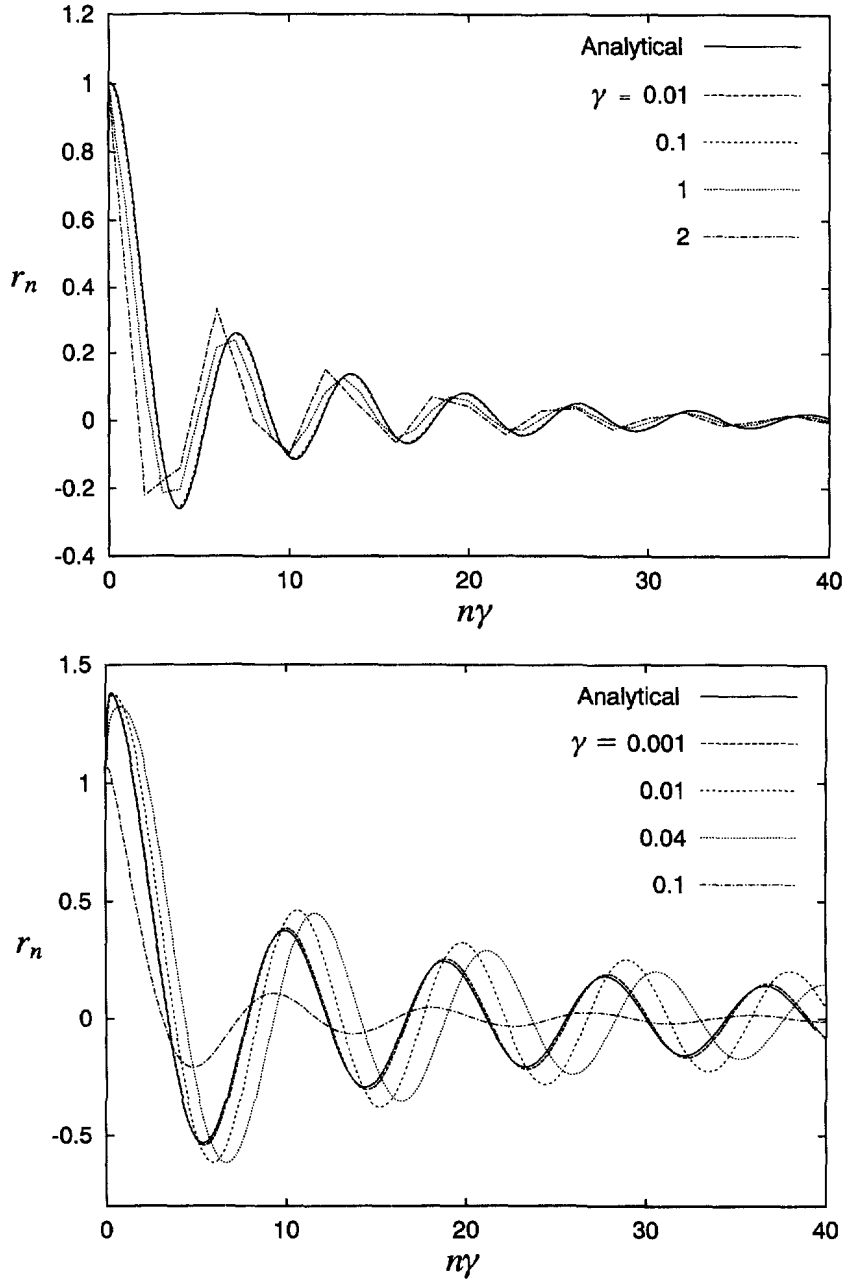

Fig. 6. Effect of γ on the numerical solution of the modal problem for $\xi = 1.0$, $b = 0.1$ (a), and $b = 10$ (b).

$$d_{n+1} = d_n + r_n. \tag{46}$$

Figures 6a and 6b present a comparison between the analytical and numerical solutions for the non-zero modes for $b = 0.1$ and 10.0, respectively. In each case, the precision of the numerical scheme decreases as γ increases, since a higher γ corresponds to a larger value of Δt in the discretized time-convolution integral (43) and in the time-stepping scheme (46). For large values of γ, the numerical method becomes unstable and stability limit (i.e., the maximum value of γ for which the numerical scheme remains stable) decreases as b increases.

The quantify the precision associated with each mode and with each time step, we define a precision factor P_5 as the ratio of the numerical value of the peak of $r(t)$ during the 5th period of oscillation to the corresponding analytical one derived from (40) and (41). A value of P_5 less than 1 corresponds to numerical overdamping of the solution, while a

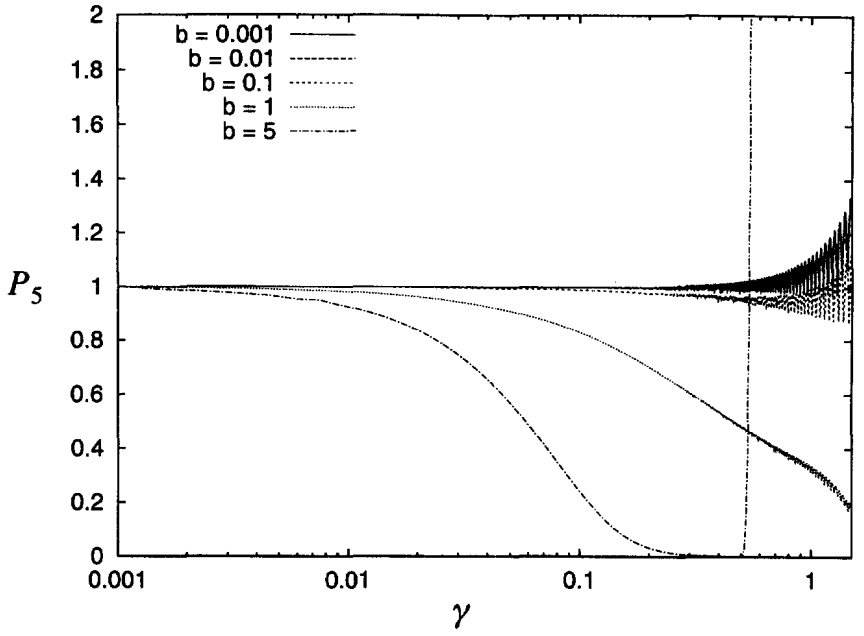

Fig. 7. Precision of the spectral scheme for various values of γ and b.

ratio greater that none is usually indicative of the onset of an unstable solution. The variation of P_5 with respect to γ is given in Fig. 7 for the various values of b, showing how the two nondimensional parameters γ and b affect the precision and stability of the numerical scheme.

The modal analysis for the constant mode ($q = 0$) corresponds to the sudden uniform anti-plane shear loading of an infinite viscoelastic half-plane. The methodology used in this case is similar to that of the other modes, even though the velocity response is quite different. As illustrated below, the 0th mode velocity response does not vanish for large times, but tends to a finite value. A precise capture of this mode is therefore essential. The analytical solution for the 0th mode is

$$r^o(t) = g^0\left(\frac{t}{\tau}\right), \tag{47}$$

where

$$g^o(T) = \mathscr{L}^{-1}\left[\frac{1}{s}\sqrt{\frac{s+1+\xi}{s+\xi}}\right]$$

$$= e^{-[\xi+(1/2)]T} I_o\left(-\frac{T}{2}\right) + (1+\xi)\int_0^T e^{-[\xi+(1/2)]u} I_o\left(-\frac{u}{2}\right) \mathrm{d}u, \tag{48}$$

where I_o is a modified Bessel function.

The corresponding numerical implementation is given by

$$r_n^o = 1 + \frac{\xi\zeta}{2} d_n - \zeta^2 \sum_{j=1}^{n} Q_j d_{n+1-j}, \tag{49}$$

where

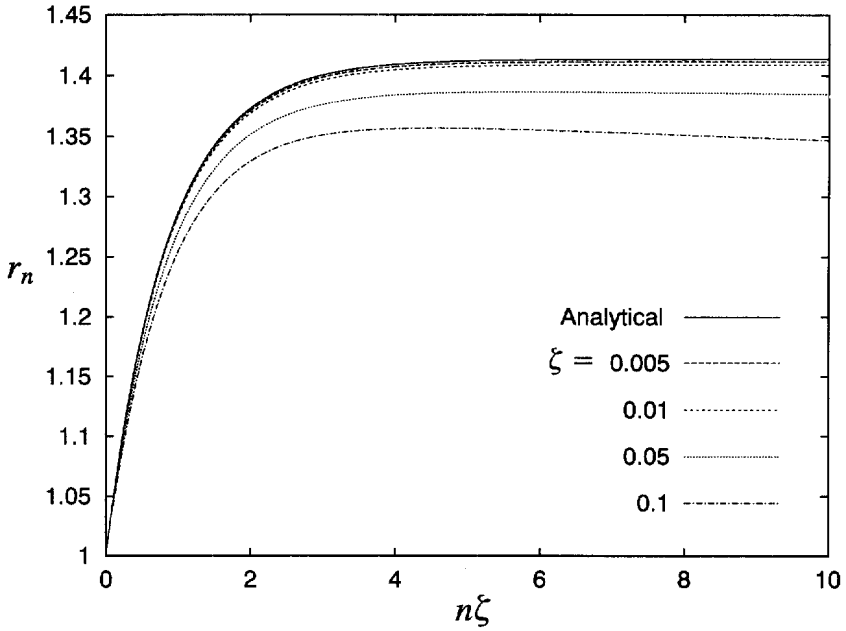

Fig. 8. Modal analysis for the zeroth mode: surface response of an infinite viscoelastic half space under a sudden uniform anti-plane shear load for various values of ζ.

$$Q_j = \tfrac{1}{2}[C_o^{ve}((j-1)\zeta) + C_o^{ve}(j\zeta)], \tag{50}$$

and ζ is the only relevant nondimensional parameter and is defined in (45), and $C_o^{ve}(T)$ is described by (34).

The numerical and analytical modal solutions for the constant mode are compared in Fig. 8. As the time step size Δt increases, the precision of the numerical scheme decreases. If one measures the precision of the scheme as the ratio of the numerical and analytical asymptotic values of $r(t)$ (Fig. 8), a value of $\zeta \leqslant 0.02$ guarantees a numerical error of less than 1% in the constant mode solution. This condition will determine the value of the time step Δt to be used in practical simulations, as described in the next section dedicated to the simulation of dynamically loaded non-propagating mode III cracks.

5. SUDDEN MODE III LOADING OF A STATIONARY CRACK

As a first application of the viscoelastodynamic spectral scheme, the classical problem of a finite-size crack of length $2a$ subjected to a sudden uniform constant anti-plane shear loading τ_o is examined. The pre-existing crack is defined as the portion of the line $x_2 = 0$ with zero strength and is prevented from propagating by assigning a very high failure strength to the part of the fracture plane located outside of the crack. In order to reduce the influence on the local stress field of the neighboring cracks associated with the spatial repetition of the fracture event, the length of the crack is chosen as $X/4$, where X is the discretized portion of the fraction plane. Based on the classical static solution of a periodic array of colinear cracks, the influence of the neighboring cracks on the stress field in the vicinity of the crack tip (i.e., on the long-time value of stress intensity factor) is then expected to be less than 4%. A total of 256 spacings of length Δx are used to discretize the crack, and the time step Δt is chosen as $\Delta x/2c_{so}$ (i.e., it takes 2 time steps for the elastic shear wave to propagate one spacing length). The evolution of the slip displacement and velocity at the center of the crack is presented in Figs 9a and 9b, respectively, in the linearly elastic case (solid curves) and for five values of the relaxation time τ (dashed curves).

As expected, during the initial times of the simulation ($0 \leqslant c_{so}t/a \leqslant 1$), the center point is unaware of the finite size of the crack and its response corresponds to that of an infinite crack under uniform loading, until the waves emanating from the crack tips reach the center

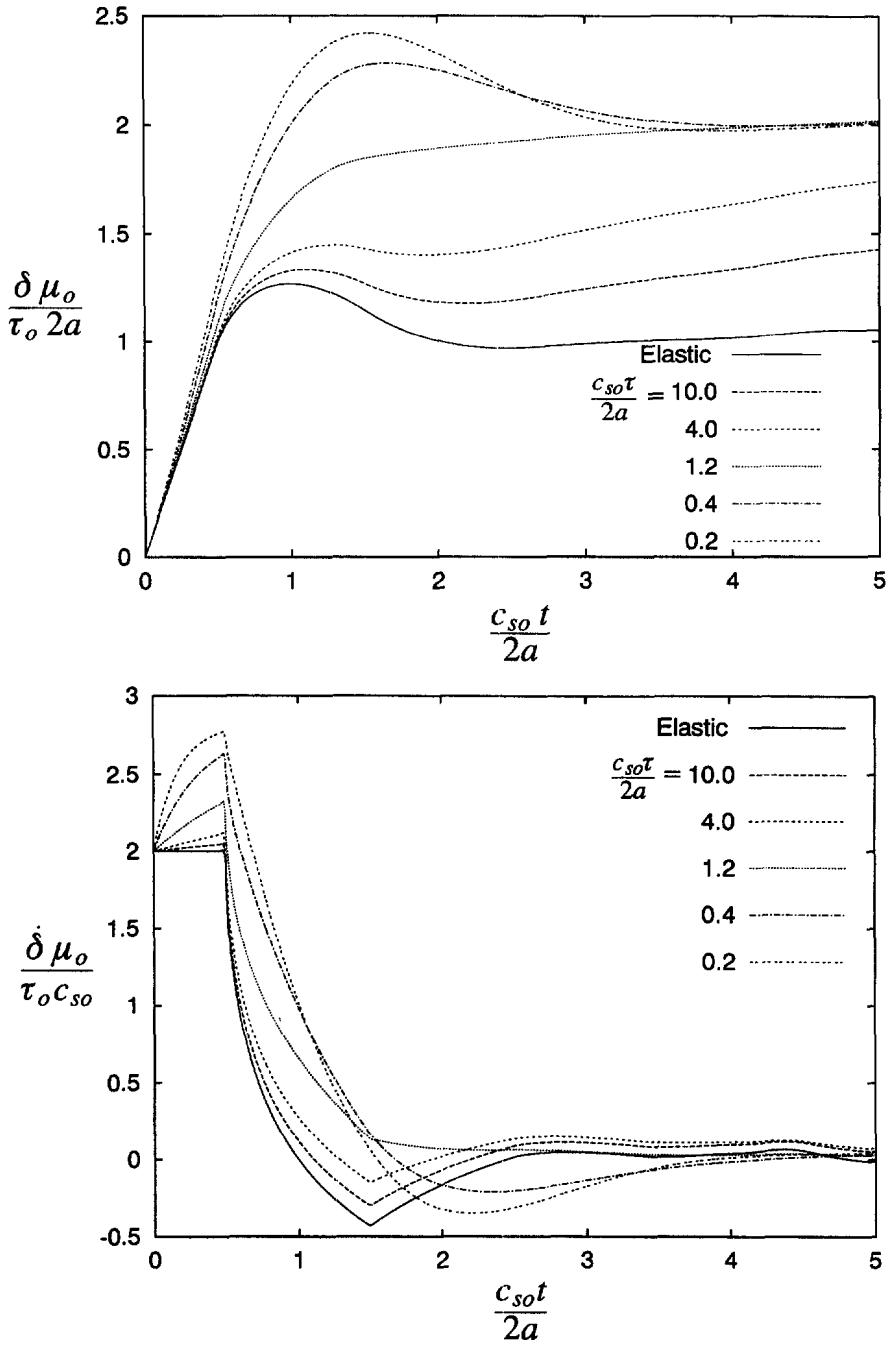

Fig. 9. Evolution of the displacement discontinuity δ (a) and slip velocity $\dot{\delta}$ (b) at the center of a finite crack of length $2a$ subjected to a sudden uniform mode III loading τ_o, in the linearly elastic case (solid curves) and for five viscoelastic situations ($\xi = 1$) (dashed curves).

point and progressively reduce the velocity to zero. This elastodynamic effect, symbolized by the solid curves, is also characterized by the so-called dynamic overshoot in which the displacement discontinuity reaches a maximum at $c_{so}t = 2a$, before approaching the static limit.

Figure 9 clearly illustrates how the material time-dependent behavior affects the dynamic fracture response. When the relaxation time τ is much larger than the "elastodynamic time" (defined as the time of travel of a shear wave along the crack), the aforementioned elastodynamic effects taken place well before any material relaxation

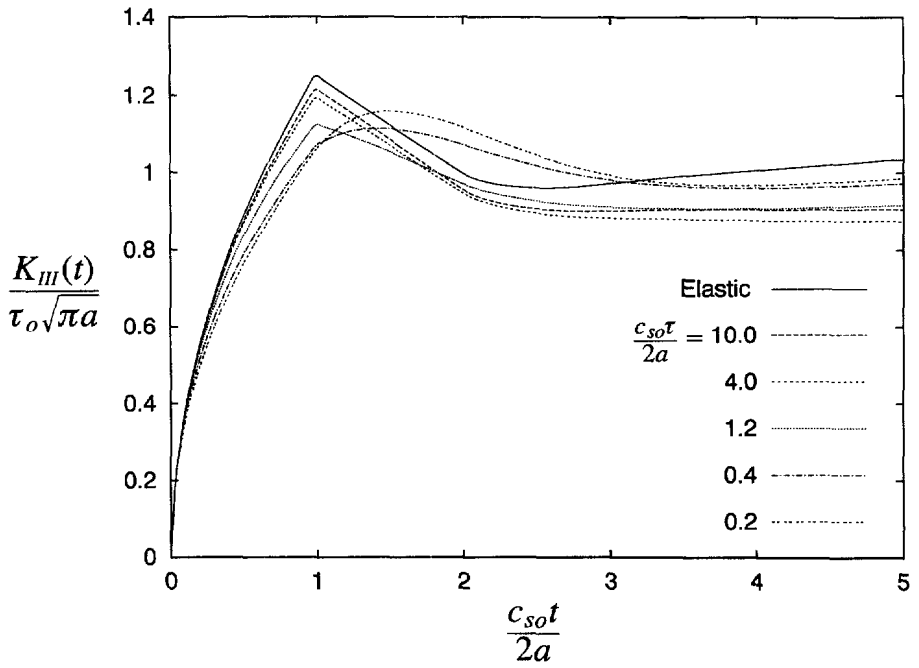

Fig. 10. Evolution of the mode III dynamic stress intensity factor $K_{III}^{ve}(t)$ for the problem shown in Fig. 9, showing the influence of the material relaxation on the dynamic overshoot ($\xi = 1$).

occurs; the dynamic response is essentially linearly elastic and the relaxation occurs quasi-statically. However, for smaller τ values, the viscous and elastodynamic effects occur simultaneously and the overall response is quite different; the material relaxation takes place before the arrival of the crack-tip waves. Furthermore, if these initial waves travel at the same velocity c_{so} as in the linearly elastic situation (and therefore hit the center point at the same time), the constantly changing shear modulus generates a whole "train" of shear waves with different velocities, thereby greatly reducing the effects of subsequent wave reflections.

The spectral method has been shown (Morrissey and Geubelle, 1997) to be a simple and efficient tool to extract the dynamic elastic stress intensity factor $K_{III}^{el}(t)$ characterizing the near-tip stress singularity. In the viscoelastic case, $K_{III}^{ve}(t)$ can be obtained by use of the elastic–viscoelastic analogy (Hilton, 1964) and is given by

$$K_{III}^{ve}(t) = \lim_{r\to 0}\left[\frac{1}{4}\sqrt{\frac{2\pi}{r}}\int_0^t \dot{\delta}(t-t')\mu(t')\,dt'\right], \tag{51}$$

where $\mu(t)$ has been defined in (6) and r is the distance to the crack tip. The evaluation of the stress intensity factor computed at the left crack tip is illustrated in Fig. 10 in the linearly elastic case (solid curve) and for the five relaxation times τ used in Fig. 9 (dashed curves). The stress intensity factor is normalized by the static elastic value $K_{III}^{el}(\infty) = \tau_o\sqrt{\pi a}$. Material relaxation reduces the dynamic overshoot and shifts it to higher time values. It also softens the effect of the unloading wave originating from the right crack tip. Note that, from (21) with $\xi = 1$, the shear modulus is within 5% of its fully relaxed value for $t/\tau > 1.5$.

6. PROPAGATING MODE III CRACK

As was mentioned in the introduction, the spontaneous propagation of cracks in a viscoelastic material is characterized by the "competition" between two energy absorption mechanisms: the viscoelastic dissipation and the creation of new surfaces. Willis (1967) has shown that viscoelasticity has an effect on crack propagation behavior, and especially, on the value of the limiting crack velocity. Due to the material-related energy dissipation, the

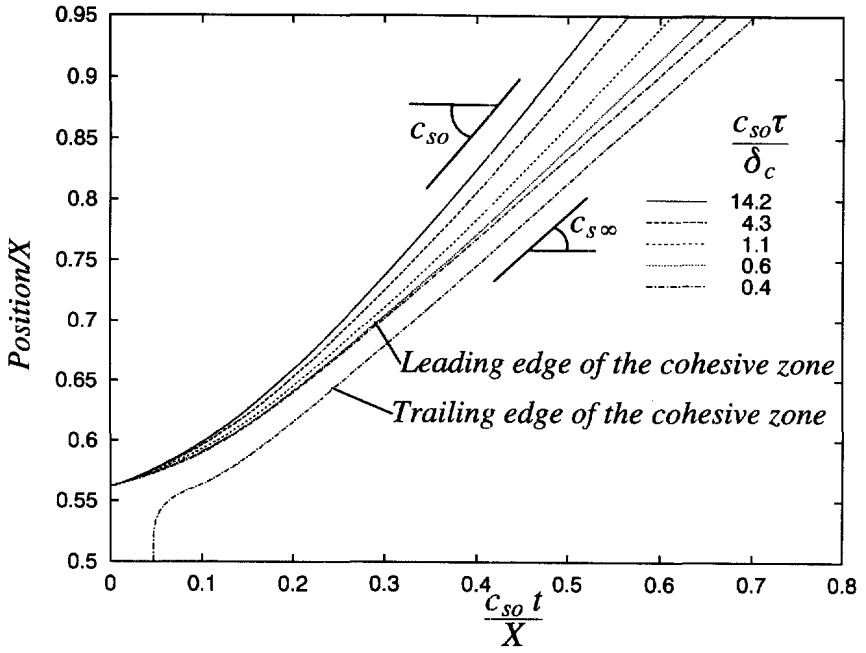

Fig. 11. Spontaneous mode III crack propagation: position of the leading edge of the cohesive zone versus time showing the influence of the relaxation constant τ on the limiting crack velocity in a SLS (with $\xi = 1$). The position of the trailing edge of the cohesive zone is also shown for the smallest value of $c_{so}\tau$, showing a similar limiting speed.

maximum crack velocity in the viscoelastic case is predicted to be smaller than its elastic counterpart, the (elastic) shear wave speed.

The spectral method presented here is a very efficient tool to investigate the spontaneous propagation of fast cracks, by allowing for the incorporation of a wide range of cohesive models to characterize the failure process in the vicinity of the traveling crack tips. In this preliminary paper dedicated to the anti-plane shear viscoelastodynamic fracture problem, the cohesive model is assumed to be rate-independent, and a simple linear cohesive law similar to that introduced in Geubelle and Rice (1995) is used. The rate-dependent effects of the failure model on the overall propagation behaviour will be examined in a subsequent paper. The failure process is thus modeled by a linear relationship between the slip and the strength, starting with an initial value of τ_c at $\delta = 0$ and progressing to a critical crack opening displacement $\delta = \delta_c$, beyond which the material is assumed to have completely failed and is unable to sustain any additional load. The energy needed to generate a new surface is then given by the area under the strength/slip curve, i.e., $\tau_c\delta_c/2$.

In order to characterize the viscoelastic effect on the limiting velocity v_{limit} of a propagation mode III crack, a series of simulations have been performed in which a constant traction $\tau_o = 0.6\tau_c$ is uniformly applied along the spontaneously expanding fracture surface in a viscoelastic medium with varying relaxation times τ. The evolution of the position of the leading edge of the right cohesive zone, i.e., the right-most point for which the displacement discontinuity δ is non-zero, is presented in Fig. 11. In the description that follows, the leading edge of the cohesive zone was chosen as location of the crack tip, thereby defining the extent of the uniform applied loading. As is apparent in Fig. 11, the crack accelerated and quickly reached a steady-state regime in which a balance was achieved between the energy associated with the uniform loading of the crack faces and that corresponding to the creation of new surfaces, the emission of acoustic waves, and viscoelastic dissipation. The evolution of the trailing edge of the cohesive zone, i.e., the right-most point for which $\delta = \delta_c$, is only shown in the case $c_{so}\tau = 0.4\,\delta_c$ for clarity purpose. Its behavior is similar to that obtained by Yang and Ravi-Chandar (1995) in their detailed finite difference analysis of spontaneous mode III crack propagation in linearly elastic materials: during the initial transient part of the simulation, the trailing edge of the cohesive zone stays stationary until

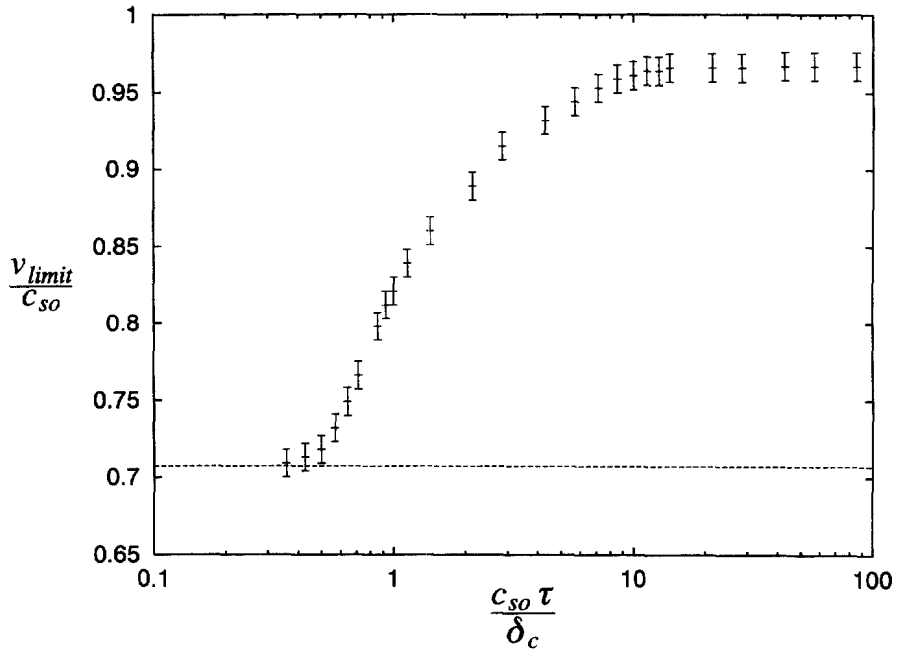

Fig. 12. Variation of the limiting crack tip velocity with respect to the relaxation time τ ($\xi = 1$).

sufficient crack opening is achieved. Then, it accelerates very rapidly and "catches up" with the leading edge.

As mentioned in the section dedicated to the numerical implementation, the spectral scheme is based on a fixed uniform spatial discretization. This implies that the spontaneous crack propagation takes place in a step-like fashion, the crack tip pausing for a few time steps before "jumping" by one element spacing Δx. The associated transient effects do not however seem to affect the numerical solution when a fine spatial discretization is adopted, as is the case here where spatial 1024 elements were used to discretize the portion X of the fracture plane. As was the case in the previous problem, the time step was chosen as $\Delta t = \Delta x/2c_{so}$. In order to accurately capture the cohesive failure, the critical crack opening displacement δ_c was chosen so as to ensure that there would be at least 15 spacing lengths Δx in the cohesive zone behind the crack tip.

The viscoelastic simulations range between the elastic limiting values $v_{\text{limit}} = c_{so} = \sqrt{\mu_o/\rho}$ corresponding to the initial modulus and $v_{\text{limit}} = c_{s\infty} = \sqrt{\mu_\infty/\rho}$ associated with the fully relaxed material. In this particular series of simulations, ξ was chosen as 1 (corresponding to $\mu_o/\mu_\infty = 2$), yielding $c_{s\infty}/c_{so} = 1/\sqrt{2}$. Variations of the limiting velocity with respect to relaxation time is illustrated in Fig. 12. The error bars depict the imprecision associated with the computation of the slope of the curves presented in Fig. 11. Note that, even in the elastic limit, the limiting crack velocity is always slightly less than the predicted value c_{so}. This is due to the fact that the crack velocity only approaches the wave speed asymptotically (Freund, 1990). Furthermore, the size of the cohesive zone is then expected to shrink to zero, which would make it impossible for this numerical scheme to capture the failure process. As shown in Fig. 12, the material dissipation only affects the propagation behavior of the crack for fairly small values of the relaxation constant ($c_{so}\tau/\delta_c \leqslant 9$). For higher τ values, viscoelastic effects do not influence the energy balance that takes place in the vicinity of the crack tip, and the viscoelastic dissipation occurs well behind the moving crack tip. For values of $c_{so}\tau/\delta_c < 0.4$, the viscoelastic effect takes place so fast that the strain energy flowing into the moving crack tip corresponds mainly to a fully relaxed medium, yielding a limiting velocity of $c_{s\infty}$.

7. CONCLUSION

A series of dynamic fracture problems in a viscoelastic material under anti-plane shear loading conditions have been investigated using a specially developed spectral scheme. The

numerical method, which is based on an exact representation of the viscoelastodynamic relations between stresses and displacements along the fracture plane, provides a very efficient and accurate tool to simulate dynamic loading and/or spontaneous rapid propagation of cracks and faults, and allows to precisely assess the influence of the viscoelastic dissipation on the overall dynamic fracture behavior of the material.

Using the simpler framework of the anti-plane shear (mode III) problem, this paper has emphasized the major differences existing between the elastic and viscoelastic spectral formulations, and the effects of these differences on the stability and precision of the associated numerical schemes. The main distinction between the two problems is the appearance of a different viscoelastodynamic convolution kernel for each spectral mode, implying additional computation and storage requirements.

Among the conclusions of the problems investigated in this paper are:

(1) The strong effect of viscoelastic material behavior on the evolution of the near-tip field, affecting dynamic overshoot of the stress intensity factor.

(2) The influence of the material dissipation on the energy balance taking place at the tip of a spontaneously propagating mode III crack, yielding a limiting crack velocity value inferior to its elastic counterpart.

REFERENCES

Atkinson, C. and List, R. D. (1972) A moving crack problem in a viscoelastic solid. *International Journal of Engineering Science* **10,** 309–322.

Atkinson, C. and Popelar, C. H. (1979) Antiplane dynamic crack propagation in a viscoelastic strip. *Journal of the Mechanics and Physics of Solids* **27,** 431–439.

Bourne, J. P. and Walton, J. R. (1993) On a dynamically accelerating crack in an Achenbach–Chao viscoelastic solid. *International Journal of Engineering Science* **31,** 569–581.

Chen, E. P. and Sih, G. C. (1977) Transient response of cracks to impact. In *Elastodynamic Crack Problems*, ed. G. C. Sih. Noordhoff Publishing, Leyden, pp. 1–58.

Cochard, A. and Rice, J. R. (1996) A spectral method for elastodynamic fracture analysis without spatial replication of the rupture event. *Journal of the Mechanics and Physics of Solids* (to appear).

Crump, K. S. (1976) Numerical inversion of Laplace transforms using a Fourier series approximation. *Journal of the Association of Computing Machines* **23,** 89–96.

Dubner, H. and Abate, J. (1968) Numerical inversion of Laplace transforms by relating them to the finite Fourier cosine transform. *Journal of the Association of Computing Machines* **15,** 115–123.

Freund, L. B. (1990) *Dynamic Fracture Mechanics*. Cambridge University Press, New York.

Georgiadis, H. G. (1993) Shear and torsional impact of cracked viscoelastic bodies—a numerical integral equation/transform approach. *International Journal of Solids and Structures* **30,** 1891–1906.

Georgiadis, H. G., Theocaris, P. S. and Mouskos, S. C. (1991) Plane impact of a cracked viscoelastic body. *International Journal of Engineering Science* **29,** 171–177.

Geubelle, P. H. and Rice, J. R. (1995) A spectral method for 3D elastodynamic fracture problems. *Journal of the Mechanics and Physics of Solids* **43,** 1791–1824.

Goleniewski, G. (1988) Dynamic crack growth in a viscoelastic material. *International Journal of Fracture* **37,** R39–R44.

Gottlieb, D., Shu, C. W., Solomonoff, A. and Vandeven, H. (1992) On the Gibbs phenomenon: 1. Recovering exponential accuracy from the Fourier partial sum of a non-periodic analytic function. *Journal of Computer Applied Mathematics* **43,** 81–98.

Herrmann, J. M. and Schovanec, L. (1994) Dynamic steady-state mode-III fracture in a nonhomogeneous viscoelastic body. *Acta Mechanica* **106,** 41–54.

Herrmann, J. M. and Walton, J. R. (1991) A comparison of the dynamic transient antiplane shear crack energy release rate for standard linear solid and power law type viscoelastic materials. *ASME Journal of Energy Resources Technology* **113,** 222–229.

Herrmann, J. M. and Walton, J. R. (1994) On the energy release rate for dynamic transient mode 1 crack propagation in a general linear viscoelastic body. *Quarterly Applied Mathematics* **52,** 201–228.

Hilton, H. H. (1964) Engineering design for plastics. In *An Introduction to Viscoelastic Analysis*, ed. E. Baer. Reinhold Publishing Corporation, New York, pp. 199–276.

Morrissey, J. M. and Geubelle, P. H. (1997) A numerical scheme for mode III dynamic fracture problems. *International Journal of Numerical Methods in Engineering* **40,** 1181–1196.

Perrin, G., Rice, J. R. and Zheng, G. (1994) Self-healing slip pulse on a frictional surface. *Journal of the Mechanics and Physics of Solids* **43,** 1461–1495.

Popelar, C. H. and Atkinson, C. (1980) Dynamic crack propagation of a viscoelastic strip. *Journal of the Mechanics and Physics of Solids* **28,** 79–93.

Ryvkin, M. and Banks-Sills, L. (1994) Mode III delamination of a viscoelastic strip from a dissimilar viscoelastic half-plane. *International Journal of Solids and Structures* **31,** 551–566.

Sills, L. B. and Benveniste, Y. (1981) Steady state propagation of a mode 3 interface crack in an inhomogeneous viscoelastic media. *International Journal of Engineering Science* **19,** 1255–1268.

Walton, J. R. (1982) On steady-state propagation of anti-plane shear crack in an infinite general linearly viscoelastic body. *Quarterly Applied Mathematics* **40,** 37–52.

Walton, J. R. (1995) Dynamic viscoelastic fracture. In *Crack and Contact Problems for Viscoelastic Bodies*, eds G. A. C. Graham and J. R. Walton. Springer-Verlag, Wien, New York, pp. 259–311.
Walton, J. R. and Herrmann, J. M. (1992) A new method for solving dynamically accelerating crack problems: Part 1. The case of a semi-infinite mode III crack in elastic material revisited. *Quarterly Applied Mathematics* **50,** 373–387.
Willis, J. R. (1967) Crack propagation in viscoelastic media. *Journal of the Mechanics and Physics of Solids* **15,** 229–240.
Yang, B. and Ravi-Chandar, K. (1996) On the role of the process zone in dynamic fracture. *Journal of the Mechanics and Physics of Solids* **44,** 1955–1976.

APPENDIX

We summarize here the mode III spectral formulation for a general class of viscoelastic materials characterized by the Prony series expression (6) of the relaxation modulus in shear. The associated dimensionless Laplace transform shear modulus $\hat{m}(p)$ is then given by

$$\hat{m}(p) = 1 - \sum_{n=1}^{\infty} \frac{\mu_n}{\mu_o \tau_n} \frac{1}{p + 1/\tau_n}. \tag{A.1}$$

The convolution kernel $R_{\mathrm{III}}^{ve}(T)$ appearing in (20) is expressed as

$$R_{\mathrm{III}}^{ve}(T) = \mathscr{L}^{-1}[\hat{R}_{\mathrm{III}}^{ve}(s)] = \mathscr{L}^{-1}\left[\hat{m}(s)\sqrt{1 + \frac{s^2}{\hat{m}(s)}} - s\right], \tag{A.2}$$

where

$$\hat{m}(s) = 1 - \sum_{n=1}^{N} \frac{\mu_n}{\mu_o} \frac{b_n}{s + b_n}. \tag{A.3}$$

In the latter, both $s = p/|q|c_{so}$ and $b_n = 1/|q|c_{so}\tau_n$ are non-dimensional.

As was the case before, the actual viscoelastodynamic mode III convolution kernel $C_{\mathrm{III}}^{ve}(T)$ is obtained by extracting the limiting value of $\hat{R}_{\mathrm{III}}^{ve}(s)$

$$\hat{C}_{\mathrm{III}}^{ve}(s) = \hat{R}_{\mathrm{III}}^{ve}(s) - \lim_{s \to \infty} \hat{R}_{\mathrm{III}}^{ve}(s). \tag{A.4}$$

It can be readily shown that

$$\lim_{s \to \infty} \hat{R}_{\mathrm{III}}^{ve}(s) = \frac{-1}{2|q|c_{so}\tau^*} \sum_{n=1}^{N} \frac{\mu_n}{\mu_o} \frac{\tau^*}{\tau_n}, \tag{A.5}$$

where τ^* is the arbitrarily chosen reference relaxation time of the viscoelastic material. The final expression of the viscoelastodynamic spectral relations is thus

$$\tau_3(x_1, t) = \tau_3^0(x_1, t) - \frac{\mu_o}{2c_{so}} \dot{\delta}(x_1, t) + W\delta(x_1, t) + f(x_1, t), \tag{A.6}$$

where

$$W = \frac{\mu_o}{4c_{so}\tau^*} \sum_{n=1}^{N} \frac{\mu_n}{\mu_o} \frac{\tau^*}{\tau_n}. \tag{A.7}$$

The convolution term is again expressed in the spectral domain as

$$F(t; q) = -\frac{\mu_o |q|}{2} \int_0^t C_{\mathrm{III}}^{ve}(|q|c_{so}t') D(t - t', q) |q| c_{so}\, \mathrm{d}t', \tag{A.8}$$

for the non-zero modes, and

$$F(t; 0) = -\frac{\mu_o}{2c_{so}\tau^*} \int_0^t C_o^{ve}\left(\frac{t'}{\tau^*}\right) D(t - t'; 0) \frac{\mathrm{d}t'}{\tau^*}, \tag{A.9}$$

for the constant spectral mode. The convolution kernels appearing in (A.8) and (A.9) are given in the Laplace domain by (A.2), (A.4) and (A.5) for the non-zero modes, and by

$$\hat{C}_o^{ve}(s) = s\sqrt{1 - \sum_{n=1}^{N} \frac{\mu_n}{\mu_o} \frac{\tau^*/\tau_n}{s + \tau^*/\tau_n}} - s + \frac{1}{2} \sum_{n=1}^{N} \frac{\mu_n}{\mu_o} \frac{\tau^*}{\tau_n}. \tag{A.10}$$

The formulation for the SLS can be easily recovered by substituting $N = 1$, $\tau^* = \tau$, $\mu_1 = \mu_o\xi/(1+\xi)$ and $\tau_1 = \tau/(1+\xi)$.